

Article

Simulation of the Fatigue Crack Initiation in SAE 52100 Martensitic Hardened Bearing Steel during Rolling Contact

Kiarash Jamali Dogahe ^{1,2,*}, Vinzenz Guski ¹, Marijo Mlikota ¹, Siegfried Schmauder ¹,
Walter Holweger ^{3,4}, Joshua Spille ⁵, Joachim Mayer ⁵, Alexander Schwedt ⁵, Bernd Görlach ⁶
and Jürgen Wranik ^{4,7}

- ¹ Institute for Materials Testing, Materials Science and Strength of Materials (IMWF), University of Stuttgart, Pfaffenwaldring 32, 70569 Stuttgart, Germany; vinzenz.guski@imwf.uni-stuttgart.de (V.G.); marijo.mlikota@imwf.uni-stuttgart.de (M.M.); siegfried.schmauder@imwf.uni-stuttgart.de (S.S.)
- ² Graduate School of Advanced Manufacturing Engineering (GSaME), Nobelstraße 12, 70569 Stuttgart, Germany
- ³ Technology Consultant, Sailegärten 2, 72351 Erlaheim, Germany; walter.holweger@t-online.de
- ⁴ National Centre for Advanced Tribology at Southampton (nCATS), Mechanical Engineering Department, School of Engineering, Faculty of Engineering and Physical Sciences, University of Southampton, Southampton SO17 1BJ, UK; j.wranik@zeller-gmelin.de
- ⁵ Central Facility for Electron Microscopy (GFE), RWTH Aachen University, Ahornstraße 55, 52074 Aachen, Germany; spille@gfe.rwth-aachen.de (J.S.); mayer@gfe.rwth-aachen.de (J.M.); schwedt@gfe.rwth-aachen.de (A.S.)
- ⁶ ASC-Görlach, Robert Bosch Straße 60, 72810 Gomaringen, Germany; goerlach@hybridlayers.de
- ⁷ Zeller+Gmelin GmbH & Co. KG, Schlossstraße 20, 73054 Eisingen, Germany
- * Correspondence: kiarash.dogahe@imwf.uni-stuttgart.de



Citation: Dogahe, K.J.; Guski, V.; Mlikota, M.; Schmauder, S.; Holweger, W.; Spille, J.; Mayer, J.; Schwedt, A.; Görlach, B.; Wranik, J. Simulation of the Fatigue Crack Initiation in SAE 52100 Martensitic Hardened Bearing Steel during Rolling Contact. *Lubricants* **2022**, *10*, 62. <https://doi.org/10.3390/lubricants10040062>

Received: 24 February 2022

Accepted: 31 March 2022

Published: 7 April 2022

Publisher's Note: MDPI stays neutral with regard to jurisdictional claims in published maps and institutional affiliations.



Copyright: © 2022 by the authors. Licensee MDPI, Basel, Switzerland. This article is an open access article distributed under the terms and conditions of the Creative Commons Attribution (CC BY) license (<https://creativecommons.org/licenses/by/4.0/>).

Abstract: An investigation on the White Etching Crack (WEC) phenomenon as a severe damage mode in bearing applications led to the observation that in a latent pre-damage state period, visible alterations appear on the surface of the raceway. A detailed inspection of the microstructure underneath the alterations reveals the existence of plenty of nano-sized pores in a depth range of 80 μm to 200 μm . The depth of the maximum Hertzian stress is calculated to be at 127 μm subsurface. The present study investigates the effect of these nanopores on the fatigue crack initiation in SAE 52100 martensitic hardened bearing steel. In this sense, two micro-models by means of the Finite Element Method (FEM) are developed for both a sample with and a sample without pores. The number of cycles required for the crack initiation for both samples is calculated, using the physical-based Tanaka–Mura model. It is shown that pores reduce the number of cycles in bearing application to come to an earlier transition from microstructural short cracks (MSC) to long crack (LC) propagation significantly.

Keywords: fatigue initiation time; finite element method; SAE 52100 martensitic hardened bearing steel; porosity; microstructure; physical-based model; rolling contact fatigue

1. Introduction

Bearings are part of any common drive train in various industrial and automotive applications. As a part of a drive train, they are important components in the service life cycle reliability. Bearings carry high loading magnitudes effectively and due to this aspect they need to be designed very precisely, with high reliability and durability, respectively [1].

SAE 52100 through-hardened steel is a martensitic hardened steel which, due to its high hardness, is typically used for rolling contact applications in order to withstand high cycle fatigue [2]. Plenty of investigations have been carried out in order to predict the reliability of the SAE 52100 martensitic steel in service life as a matter of its microstructure.

The effect of heat treatment on the surface fatigue crack initiation of SAE 52100 martensitic hardened steel was analyzed by Beswick [3]. Lundberg and Palmgren [4] and Ioannides and Harris [5] described predictive methods, which are used to calculate the

lifetime of the bearing components numerically. It has been proposed by Sadeghi et al. [6] and Walveker et al. [7] that for the ball and roller bearings, under proper loading condition and lubrication, correct installation of all the bearing components, and without contamination, the main cause of the failure is material fatigue phenomena. It is shown that the main reason for the limited life of bearing elements is subsurface initiated fatigue spallation and subsurface porosities [7].

Spriesterbach et al. [2] investigated the effect of inclusions with different chemical compositions and the fatigue crack initiation induced by them.

Spille et al. [8] studied the initiation processes of White Etching Cracks (WECs) on an FE8 test rig (Figure 1, Schaeffler) in SAE 52100 martensitic hardened steel.

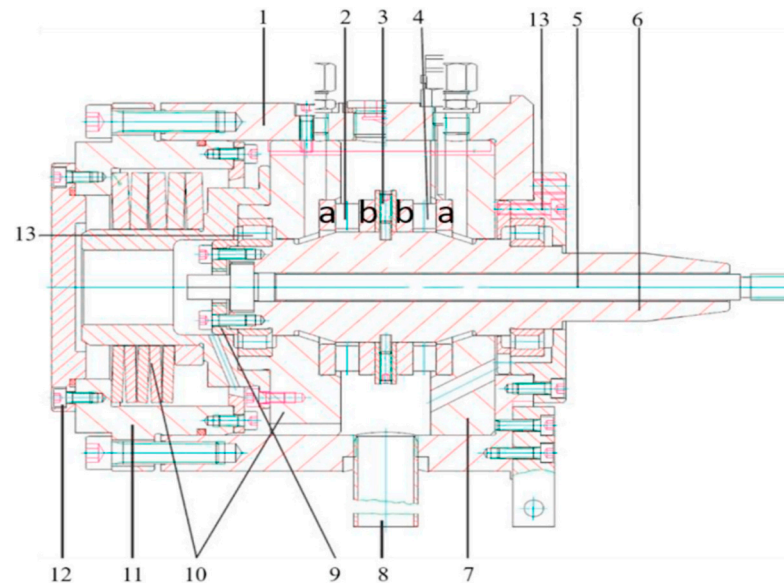


Figure 1. Test bench with axial cylindrical roller bearings. 1 housing, 2 thrust bearing 2, 3 spacer, 4 thrust bearing 1, 5 shaft, 6 clamping bolt, 7 bearing seat, 8 drain pipe, 9 cap, 10 bearing support with the screwed-on pilot pin, 11 lid cup of spring package, 12 lid, 13 auxiliary bearing. Both test bearings consist of a housing and a shaft washer. The two shaft washers (b) are mounted on the shaft and rotate during testing; the two housing washers (a) are embedded in the housing/support [8].

Generally, in order to increase the reliability of the system as well as preventing wear, which is caused by uncontrolled mixed friction especially within the contact area, the implementation of a lubricant in the test bench is necessary. However, lubrication of the component has a huge effect on its mechanical performance due to the formation of WEC caused by chemical reactions [9]. The existence of pores within the microstructure of samples that are prone to WEC formation was proven by Spille et al. [8]. Further investigations employing Electron Backscatter Diffraction (EBSD) showed microstructural changes such as the formation of new grain boundaries in area close to the pores, which has a big effect on the mechanical behaviour of the bearings, especially from a fatigue life point of view.

Another investigation of the same working bench at reference [8] is done by Holweger et al. [10]. In this work, the fatigue performance of the bearing components is investigated in two modes: Rolling Contact Fatigue (RCF) and Electrical charged Contact Fatigue (ECCF). It is observed that under the standard operating condition (called RCF), the bearing has reached up to 10^9 cycles without failure, while exposing it to a different lubricant combined with electrical charging (ECCF mode) led to spalling caused by WEC after 10^8 load cycles, proving the fact that fatigue may be severely driven by external factors rather than pure mechanical loading.

So far, all investigations on the fatigue life of roller bearings mainly focused on the propagation of existing cracks within the microstructure. In a study by Murakami et al. [11],

it is shown that due to the stress concentrations near pores, the stress values in these areas are a function of the distance from the pore surface. The value of the stress intensity factor (K) for an existing crack near a spherical pore under stress σ can be obtained by:

$$K = \sigma(\rho + a)\sqrt{\pi a}Y, \tag{1}$$

in which a is the crack length, ρ is the radius of the spherical pore, and Y is a geometry factor which is a function of a/ρ . Lai et al. [12] divided the crack growth from the edge of a spherical pore into three stages (Figure 2). In stage I, the crack is smaller than the radius of the pore and Y shows its own maximum value (orange dashed line). In stage II, Y starts to decrease by increasing the a/ρ ratio due to the beginning of crack propagation. In stage III, the crack finally behaves like a penny-shaped crack and Y approaches its minimum value (blue dashed line).

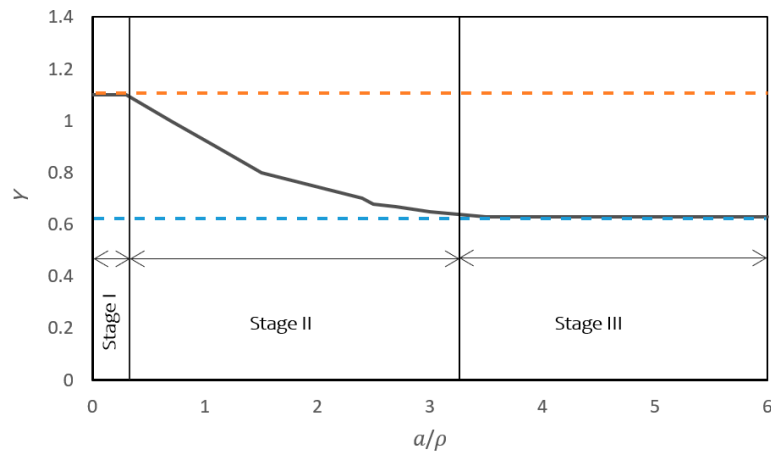


Figure 2. Geometry factor (Y) vs. a/ρ showing the three stages of crack growth from a spherical pore [12].

A conventional fatigue crack growth curve, also known as da/dN vs. ΔK curve, is shown in Figure 3. The curve is generally characterized by three stages: stage I, II, and III. It is worth mentioning that the stages I, II, and III in this sense are different with those at Figure 2.

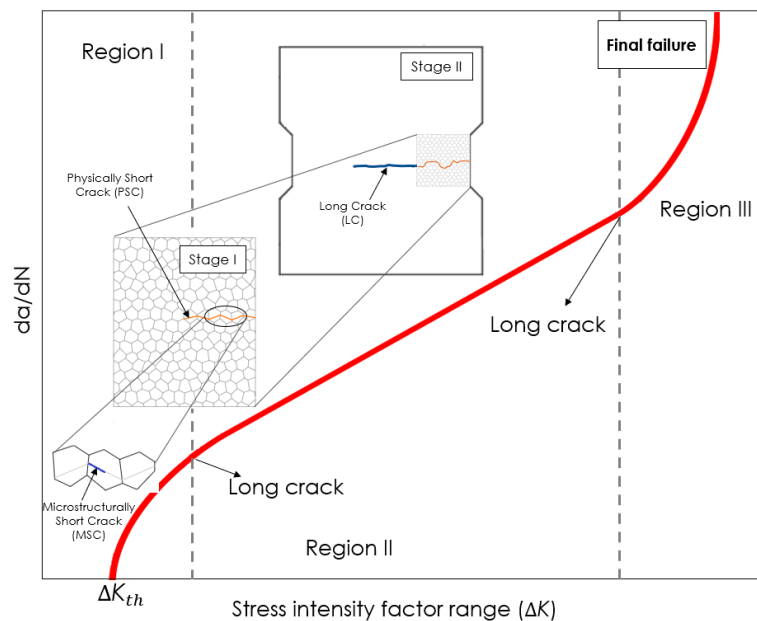


Figure 3. Schematic description of conventional fatigue crack growth behavior [13].

During the course of fatigue life, after the fatigue cracks nucleation due to the cyclic slip, within the early stages, the nucleated cracks start growing as Microstructurally Short Cracks (MSCs). In this case, the formed MSCs are in the order of the material's grain size. Due to the effect of microstructural barriers such as grain boundaries within the metallic material's microstructure, MSCs generally grow along the crystallographic planes in a disordered pattern.

After the growth of the MSCs through several grains, they are considered as Physically Short Cracks (PSCs). The material's microstructure has a big influence on the crack growth at this stage (region I).

By reaching the end of the PSC stage, the crack develops into a Long Crack (LC) in region II. In this situation, the influence of the microstructure becomes negligible, and the crack starts propagating in a continuous manner in a perpendicular direction to the loading, which continues up to the final failure in region III.

The paper presented here refers to the earlier investigations on White Etching Cracks (WECs) which is done by Holweger et al. [9], Loos et al. [14], Stadler et al. [15], and Wang et al. [16]. Although within all the mentioned investigations WEC does appear as a sudden failure, the question still remains about how it starts. So far, the experimental investigation on the WEC initiation has been kept in the investigation of Rumpf et al. [17]. The detection of the initiation of WEC is done by suspending bearings on the mentioned test rig in narrow time stamps, beginning with a determination of the failure as the first result, shown by Rumpf et al. [17].

In the present work, which is based on the experimental research work of Spille et al. [8], the authors went one step ahead, by investigating the effect of the porosities on fatigue crack initiation of SAE 52100 martensitic hardened steel in a very early damage stage with respect to the bearing components, e.g., rings, rollers, and washers. Therefore, the number of cycles for crack initiation and subsequent propagation in two assumed microstructures—with and without pores—is calculated using the physically-based Tanaka–Mura (TM) equation. Moreover, the interaction between pores and cracks is investigated. Indeed, the paper enlightens the fact that pores may lead to WEC. By pointing out the early stage key parameters, it is leading to valuable predictions for WEC in an premature stage, presumably leading to an early state counter measure.

2. Material

The investigations are carried out on the contact area between the cylinders and rings of an axial cylindrical roller bearing (type 81212; Schaeffler) (Figure 4), which is the area with the highest stress concentration. Typically, such roller bearings are applied as components in wind turbines.

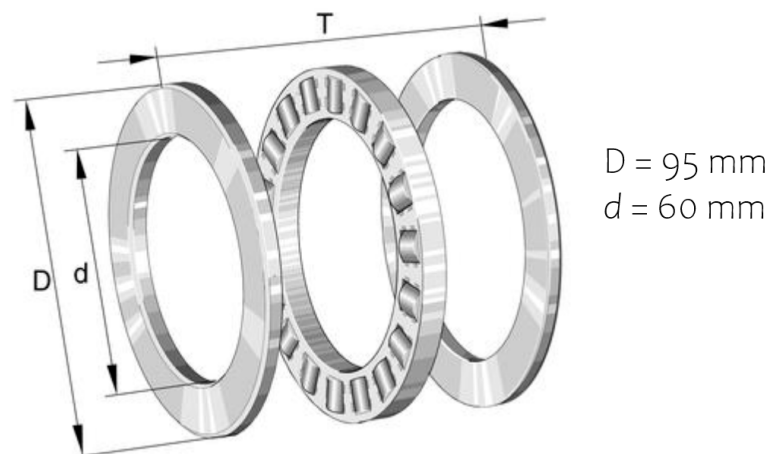


Figure 4. Axial cylindrical roller bearing (type 81212; Schaeffler).

The bearing is made of SAE 52100 martensitic hardened steel. The chemical composition is shown in Table 1. The samples were subjected to a standard heat treatment including austenitization for 20 min at 845 °C, oil quenching to 60 °C, cooling down to room temperature, and finally tempering at 180 °C for 2 h [18].

Table 1. Chemical composition of SAE 52100 martensitic hardened steel in wt % [18].

Element	C	Cr	Mn	Si	Ni	Cu	Mo	Al	S	P
Percentage	1.01	1.57	0.44	0.25	0.06	0.04	0.03	0.03	0.005	<0.01

Samples were tested on the FE8 testing (Figure 1) until the fracture occurred, then a careful material study of the failure components was done by Spille et al. [8], which led to the observation that in a pre-damaged state where no spalling was observed visible on the raceway, alterations are visible on the raceway surface (Figure 5).

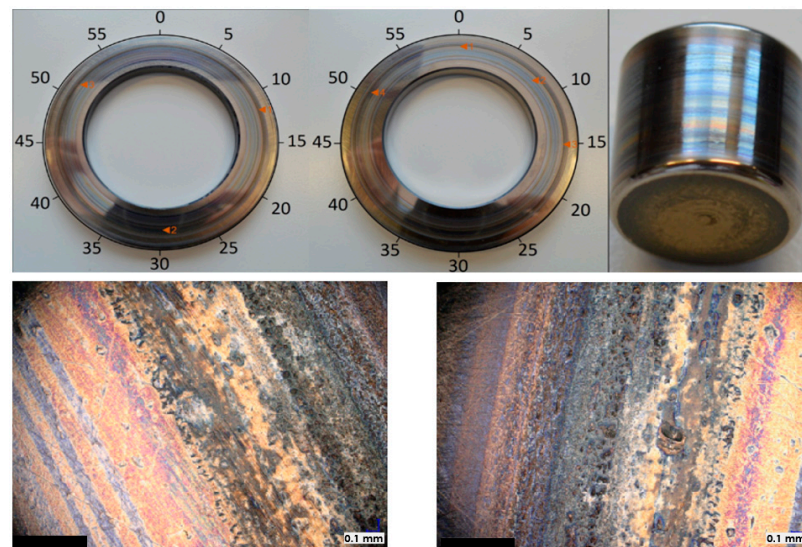


Figure 5. Alterations of the washers' surfaces from a damaged specimen.

In the sub-surface area below the alterations, seen at the raceway surface (see Figure 5) at a depth of 80–180 μm , arrays of micropores were identified together with newly formed gains and grain boundaries (here at a depth of 165 μm) as it is shown in Figure 6 (yellow circles). These observations in the experiment lead to the assumption that failure in an early stage can be related to the presence of these voids.

The S-N diagram of SAE 52100 martensitic hardened steel is shown in Figure 7 [19]. As it can be seen within the S-N diagram, the stress amplitudes below 750 MPa are under the fatigue endurance limit, and SAE 52100 martensitic hardened bearing steel is supposed to undergo an infinite number of cycles at these stress amplitudes. In order to evaluate the relevance of the voids with respect to early failures, the calculations are made on the stress amplitude level of 750 MPa.

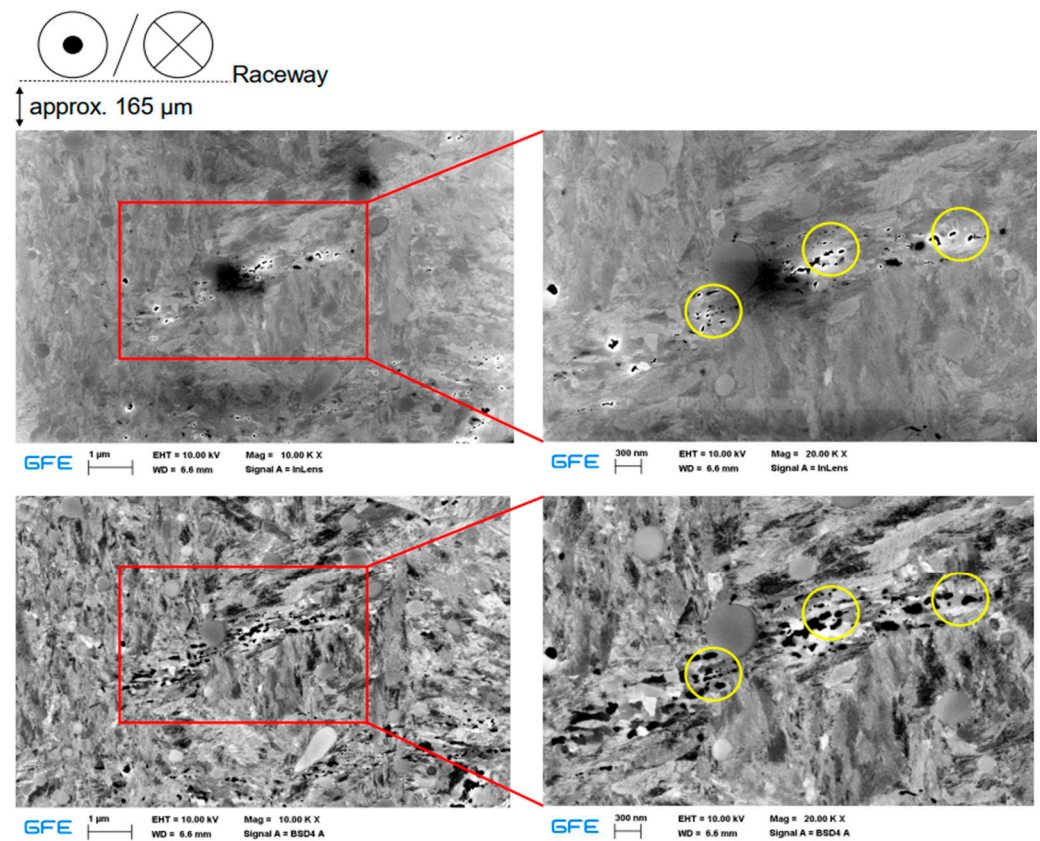


Figure 6. SE (**up**) and BSE (**down**) images of the microstructure in the depth of 165 μm below the raceway. The porosities within the microstructure are signified by the yellow circles.

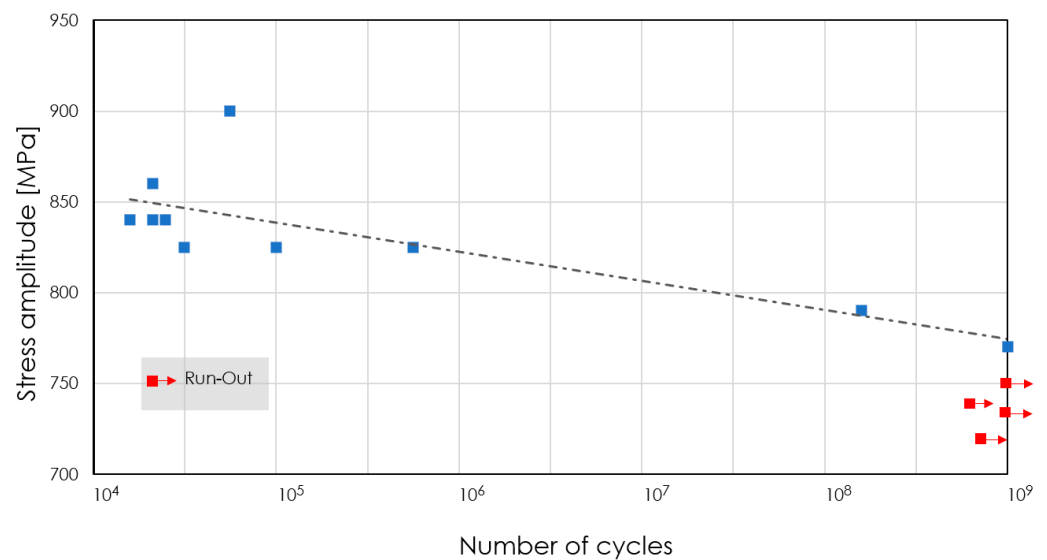


Figure 7. Experimental S-N diagram of SAE 52100 martensitic hardened steel [15].

3. Simulation

In order to calculate the required number of cycles for crack initiation under cyclic loading conditions, the physically-based Tanaka–Mura (TM) equation is employed [20,21]. The TM equation is a powerful micro-mechanical model for crack initiation on the slip band of metallic materials under cyclic loading. This method suggests an energy balance of the dislocation structure on the slip bands inside the most favorable oriented grains. The slip band consists of two series of dislocations on layers located in opposite directions to

each other, which is considered as the main factor for deformation in metallic materials as a result of forward and reverse loading (Figure 8).

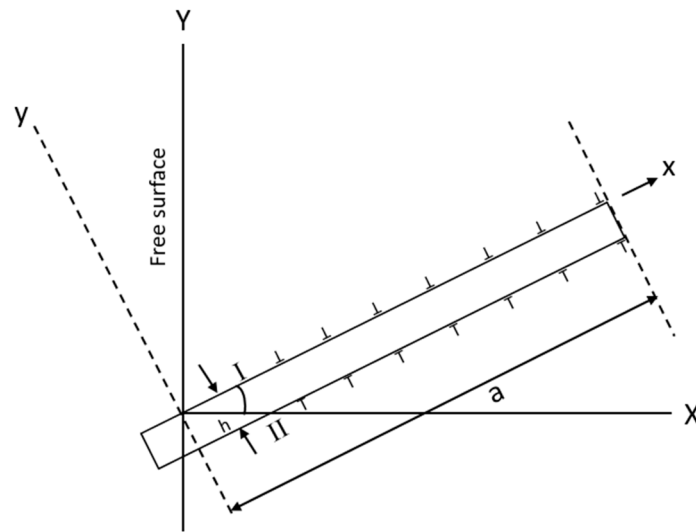


Figure 8. Schematic of a slip band as a combination of two parallel layers of dislocations colliding with a free surface at a specific angle.

The change in energy (ΔU) caused by the forwarding loading of dislocations on the layer I, to the reverse loading on layer II, is given by:

$$\Delta U = \frac{1}{2} \Delta \gamma (\Delta \tau - 2CRSS), \quad (2)$$

where $\Delta \tau$ is the average shear stress on the slip band and $CRSS$ is the critical resolved shear stress which must be exceeded for the dislocation motion. In the model $\Delta \tau > 2CRSS$ is assumed, which means that the shear stress value on the slip band should be at least twice the value of $CRSS$ to enable the dislocation movement.

The TM equation enables the calculation of the required number of cycles for crack nucleation inside grains, based on the pile-up of dislocations inside a grain under cyclic loading conditions.

$$N_s = \frac{8GW_c}{\pi(1-\nu)d_s(\Delta\tau_s - 2CRSS)^2}, \quad (3)$$

Among the parameters of Equation (3), the shear modulus (G), the Poisson's ratio (ν), the fracture energy (W_c), and particularly the critical resolved shear stress ($CRSS$) for a dislocation along with a slip band in order to start to move, are material-related parameters. These material properties can be obtained experimentally. The segment length (d_s) is a model parameter to discretize the slip bands and the average shear stress on the slip band ($\Delta\tau$) is calculated by means of finite element method (FEM) simulations.

The uniqueness of the TM model takes the contribution of the dislocation movement and the contribution of the $CRSS$, needed for their movement, into account.

Table 2 summarizes the mechanical properties of SAE 52100 martensitic hardened steel, which are required for the simulation and the TM equation (Equation (3)).

Table 2. Mechanical properties of SAE 52100 martensitic hardened steel [22,23].

E (GPa)	G (GPa)	ν	R_m (MPa)	$CRSS$ (MPa)	W_c	Slip Band Length d (μm)
210	80	0.3	962	160	69	1

Within this framework, a macro-model or so-called global model delivers the mechanical boundary conditions for the micro-models which contain the different microstructures. Regarding the material properties, an isotropic elastic behavior with Young's modulus (E)

of 210 GPa, a shear modulus (G) of 80 GPa, and a Poisson's ratio (ν) of 0.3 is assigned to the macro-model, whereas a pure elastic orthotropic behavior with material elastic constants $C_{11} = C_{22} = C_{33} = E(1 - \nu)/(1 - \nu - 2\nu^2) = 282$ GPa, $C_{12} = C_{13} = C_{23} = E\nu/(1 - \nu - 2\nu^2) = 121$ GPa, and $C_{44} = C_{55} = C_{66} = G = 80$ GPa is assigned to the micro-model. The comprehensive explanation regarding the employment of the TM formulation in FEM simulations of the crack initiation procedure is provided in the works of Mlikota et al. [24–29] and Božić et al. [30–32].

In order to apply realistic loads on the microstructure model, a two-step sub-modelling approach was employed. In this sense, a three-dimensional (3D) macro-model was developed based on Computer-Aided-Design (CAD) data of the cylindrical roller bearing shown in Figure 3. To represent operational conditions on the surface of one side of the bearing in the macro-model, a compressive load of 60 kN was applied (Figure 9), carried by 15 rolling elements, which were guided in a brass cage, resulting in a contact pressure of 1900 MPa. This load induces a stress magnitude of 750 MPa in the sub-surface area inside the ring close to the contact region, which is below the critical stress amplitude (see Figure 7). The other side of the bearing was the constraint. Between the surface of the roller and the inner surface of the rings, a tangential surface to surface contact with a friction coefficient of zero was defined. From the experimental investigations, fatigue was observed due to the dynamic contact of the roller bearings. As it can be seen in the macroscopic simulation results in Figure 9, the most critical point in the macro-model is the contact area of the cylinders and rings. Therefore, this region was selected for the subsequent sub-modelling procedure. For this purpose, a 3D FE model was generated in this area with fewer discretization. The sub-modelling procedure enables the transfer of mechanical boundary conditions to this smaller 3D FE model. This approach with an intermediate FE model is necessary to obtain an accurate stress distribution at the micro-scale with acceptable computational efforts. Finally, to perform the calculations for the fatigue crack initiation analysis, a 3D shell micro-model was developed in the critical region, which is specified in the red square in Figure 9 by repeating the sub-modelling technique in ABAQUS. The microstructure of the sample based on the cross-sections in Figure 6, is developed in the micro-model using the Voronoi tessellation technique [33,34]. An average grain size of 1.5 μm is assigned to the micro-model. The size of the micro-model was $25 \times 30 \mu\text{m}^2$ with a thickness of 0.01 μm . The generated microstructure consists of 236 grains as shown in Figure 9c. More detailed explanations regarding the sub-modelling technique employed in this work is discussed by Mlikota et al. [24,25].

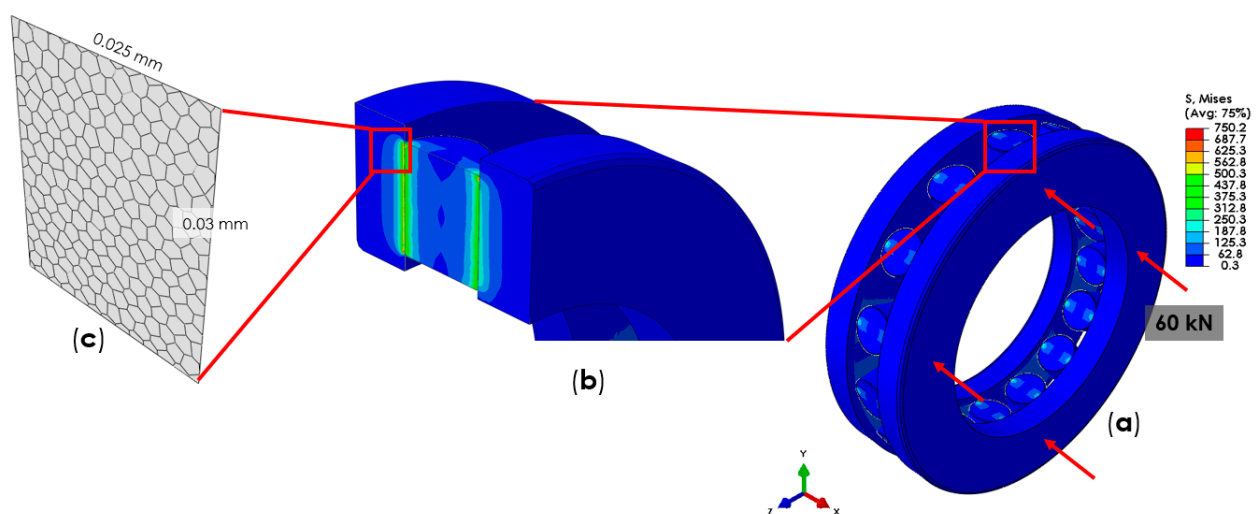


Figure 9. (a) Macro-model or global model of the bearing and the loading condition. (b) Cross-section of the macro-model in the contact area between the cylinders and the rings. (c) Micro-model developed in the area with the highest stress concentration.

In order to investigate the effect of porosity, two microstructures, with and without voids, are assigned to the micro-model, as shown in Figure 10. The voids were positioned along the grain boundaries in three grains which are located 1, 4, and 5 μm below the surface (contact face). The average radius of voids is $6 \times 10^{-2} \mu\text{m}$. Since the purpose of this numerical study was the comprehension of the effect of microstructural porosities on the fatigue behaviour of the bearing components, the position, size, and number of the voids is different from the experimental observations in order to reduce the computational time and effort. In this sense, the position of the artificial pores is considered on the grain boundaries which are the boundaries of the different sections in FEM platform. The actual number of porosities in the real microstructure is also expected to be higher, but here, in order just to get an impression about the influence of porosities on the fatigue performance of the component, 18 pores are implemented in the area with higher stress concentration. All the pores have more or less the same size in the numerical modelling.

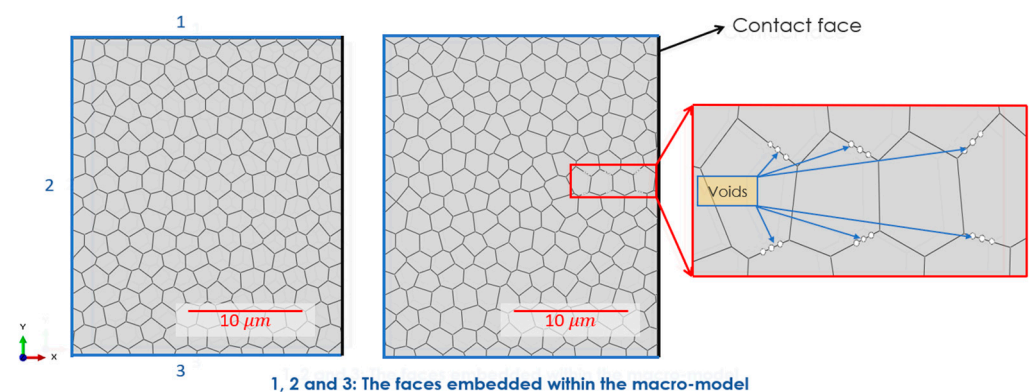


Figure 10. Microstructural models of SAE 52100 martensitic hardened steel, without pores (left) and with pores (right).

4. Results and Discussion

By applying the load on one side of the macro-model, it has been shown that the contact area between the rollers and the rings possesses the highest stress concentration (see Figure 9). Hence, the crack initiation is likely to raise from that area.

After obtaining the stress magnitudes inside the global model from a quasi-static simulation, the subsequent simulations for both microstructures with and without voids were carried out up to 50 iterations. In each step, the shear stress was evaluated and the number of cycles until crack nucleation was calculated for each segment according to Equation (3). Then the segment with the lowest number of cycles was determined and was forced to fail. Therefore, the number of cycles obtained in each iteration is the number of cycles that is required for breaking one segment inside the microstructure. In the simulation model, a microcrack appears, which changes the shear stress distribution within the model. This whole procedure was repeated until the final iteration or the transition to the next stage was reached (Figure 3). Due to the stress concentrations at the crack tips, the crack can grow. However, it is even possible that in the next step one segment belonging to another grain breaks, which depends on the grain orientations with respect to the loading condition, and if the shear stress of that segment has already surpassed the CRSS value [23].

Generally, in the current modelling approach, every MSC that is formed inside the microstructural model possesses a change of the crack length (da) and the corresponding additional cycles (formation lifetime) (dN) within an iteration. By dividing the two outputs, one can obtain the crack growth rate (da/dN) curve as a function of broken segments inside the microstructural model. As seen in Figure 11, the crack growth rate inside the microstructural model follows an oscillating pattern and drops after breaking a certain number of segments. For the model with voids, a steep drop after 36 iterations was observed (Figure 11b). This drop specifies the end of crack initiation and the beginning of the long crack (LC) propagation (region 2, see Figure 3). A similar experimental observation

regarding the descending of the short crack growth rate was reported by Newman et al. [35]. As it is depicted in Figure 3, for the short crack (PSC) growth there is a high growth rates at ΔK values, less than the LC threshold value, ΔK_{th} . By increasing the loading magnitudes as the crack length increases, the fatigue short crack data points approach towards LC curve and coincide with it [35]. For the lower stress amplitudes, the short crack even stopped growing.

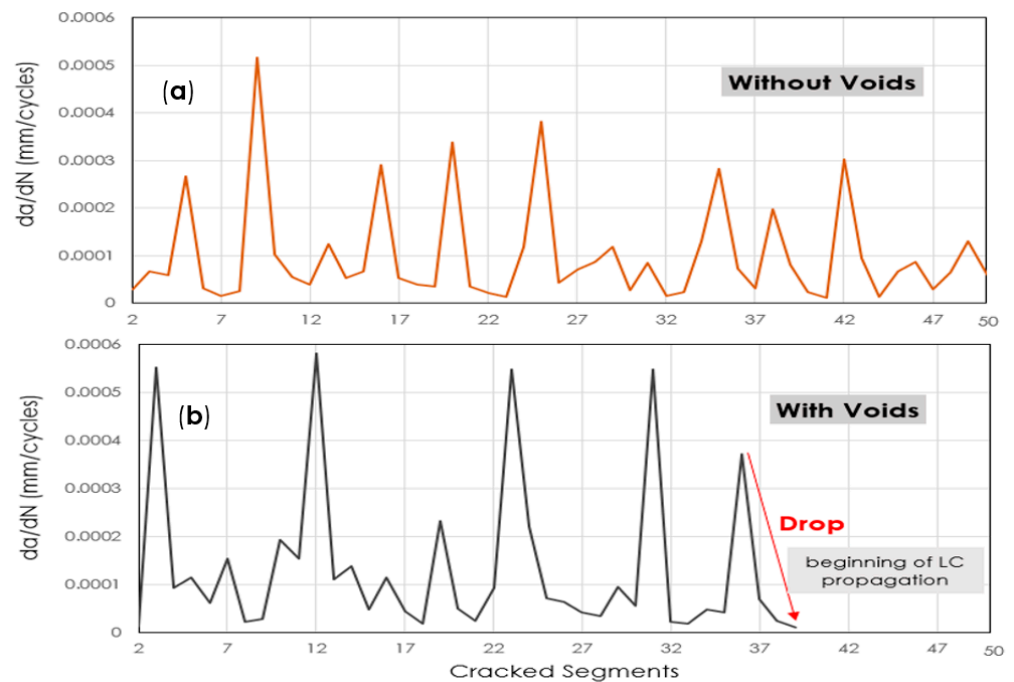


Figure 11. Comparison between fatigue crack initiation of the microstructures without voids (a) and with voids (b).

Figures 12 and 13 show the shear stress contour plot in the micro-model of the samples with and without voids for steps 1, 10, and 38 (at which the fatigue crack initiation stopped and the long crack propagation occurs for the microstructure with voids). This happens when no more micro-cracks can be formed based on the TM equation (Equation (3)), due to the higher actual shear stress distribution inside the microstructure. It was noticed that due to the transfer of the mechanical boundary conditions from the global model to the microstructure model the stresses increased strongly, which was related to a numerical artefact. Obviously, this artificial high-stress level leads to a decrease in the calculated fatigue lifetime compared to experimental values. However, both microstructural simulations show the same numerical effect. Thus, at least a qualitative comparison of the effect of porosity is reasonable.

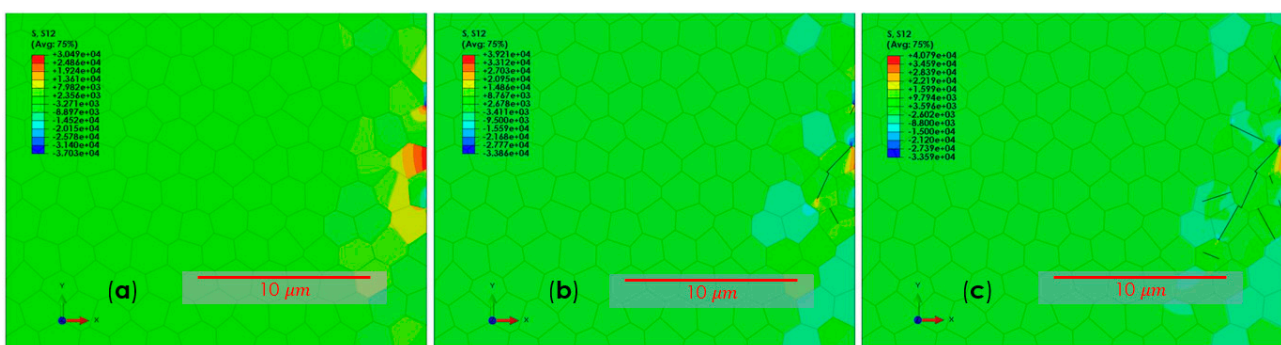


Figure 12. Damage initiation in the microstructural model of SAE 52100 martensitic hardened steel without voids in steps 1 (a), 10 (b), and 36 (c).

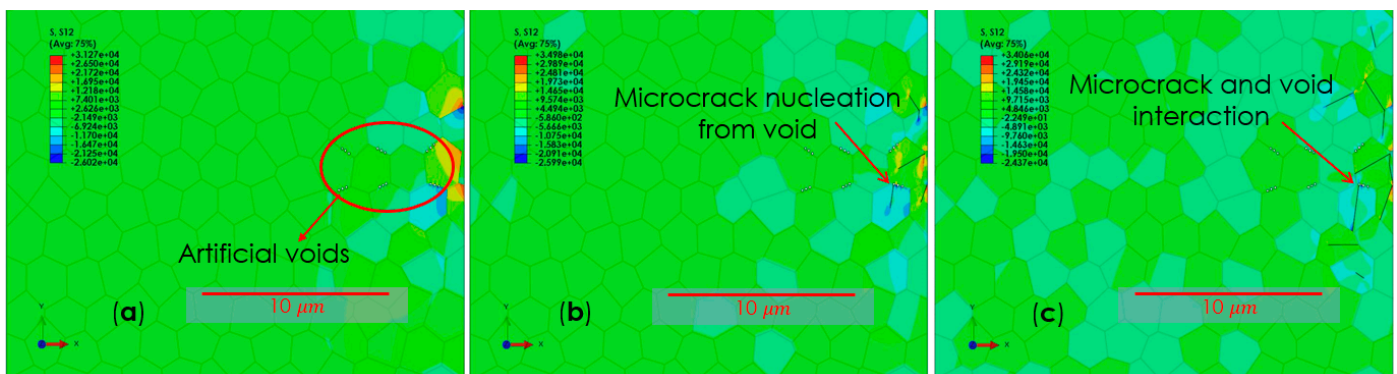


Figure 13. Damage initiation in the microstructural model of SAE 52100 martensitic hardened steel with voids in steps 1 (a), 10 (b), and 38 (c).

As can be seen in Figures 12 and 13, the voids have a strong effect on the damage initiation pattern within the subsurface microstructure. Although the shear stress magnitude at the beginning was almost equal for both structures, it is visible that the shear stress attains higher values in the microstructure without voids in comparison to the microstructure with voids. This leads to the conclusion that the initiation of the same number of cracks, in the presence of voids within the microstructure, lowers the shear stress values that are required. Moreover, the crack initiation in the location given by the voids is clearly observable (Figure 13b), continuing until the end of the procedure (Figure 13c). It is observed that the crack pattern for the model without pores has a clear path that starts from the surface area, which possesses the highest stress magnitudes. On the other hand, for the microstructure with pores, since the porosities are the potential places for stress concentration, the crack initiation can also happen subsurface inside the microstructure.

To be able to analyze the effect of the pores on the fatigue behavior, the number of calculated cycles according to Equation (3) were accumulated and plotted against and the number of failed segments, which represent the microcracks. Figure 14 shows the comparison between the two microstructures (with and without voids) with respect to the microcrack nucleation cycles.

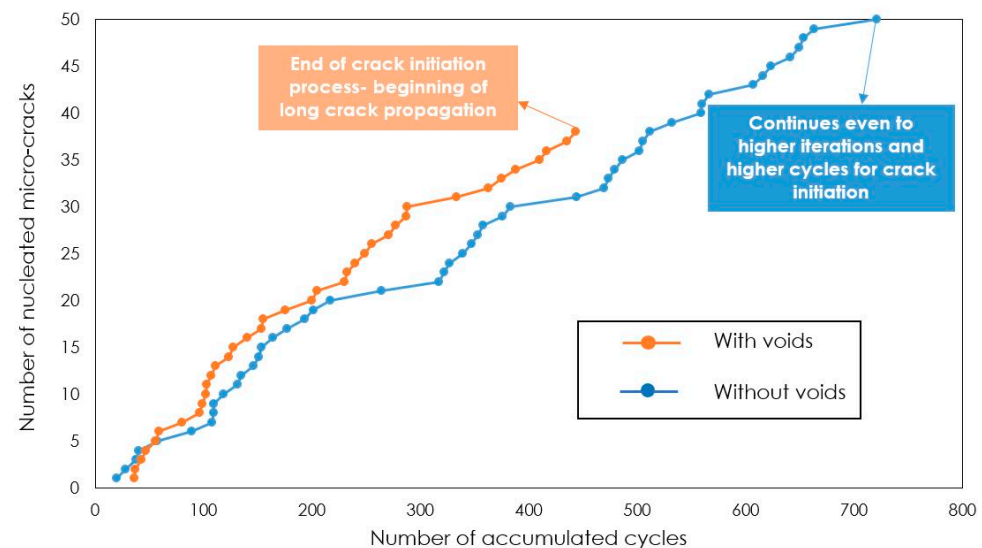


Figure 14. Comparison of the cycle accumulation for microstructures with and without voids.

As can be seen in Figure 14, voids have a significant effect on the fatigue crack initiation, especially from a cycle accumulation point of view. From the calculations, it has been observed that by increasing the number of nucleating microcracks, the differences between the results of the models with and without pores increase.

As it has been mentioned earlier, the drop for the microstructure, which includes voids happens at the 36th iteration, and the simulation process stops completely at the 38th iteration, while the simulation for the microstructure without voids continues until the end of the 50th iteration. Of course, the modelling for the microstructure without voids could continue even to higher modelling iterations, but the number of iterations for this modeling is confined to 50.

In this case, the sample without voids experienced a higher number of accumulated cycles (512 cycles) at the end of the 38th iteration in comparison to the sample with voids (443 cycles). It should also be noted that at the end of the 50th iteration, the microstructure without voids has undergone 721 accumulation cycles altogether.

This means that the presence of pores in the microstructure, even under ideal conditions (e.g., friction coefficient to be zero as assumed), significantly decreases the fatigue initiation lifetime and accelerates the beginning of long fatigue crack propagation and final failure consequently. Based on the S-N diagram of the SAE 52100 martensitic hardened steel (Figure 7), it is anticipated that the bearing component without porosities in the current loading condition (under the stress of 750 MPa) undergoes an infinite number of cycles, as it is seen also in experimental observations [10], while in the presence of porosities the S-N curve shifts downwards and the failure for the specific stress amplitude occurs at the lesser number of cycles.

5. Conclusions

In the present study, a two-step sub-modelling approach was carried out to investigate the fatigue behavior of SAE 52100 martensitic hardened steel in roller bearing contact. In particular, the influence of pores on fatigue behavior was addressed. This study is based on the assumptions that during operation voids appear in the subsurface, which influence the component lifetime. The numerical analysis performed in this work is in qualitative agreement with the experimental observations [1–3,36,37]. Apart from the experimental studies, the simulations based on the physically-based TM equation demonstrated that porosities have an influence on the shear stress distribution in the microstructural model, and also on microcrack nucleation sites, which are more distributed. Apart from that, it has also been observed that the presence of porosities inside the microstructure leads to an earlier transition to the LC propagation, which evokes the final failure of the component. Besides, the accumulation of all calculated cycles indicates a clear decrease of fatigue lifetime due to the presence of porosities. Considering these entire facts, one can conclude that the simulation results support the hypothesis about the influence of porosities on reducing the number of cycles required for microcrack nucleation and initiation of short cracks. However, for a quantitative statement on the fatigue lifetime, further investigations based on the sub-modelling technique are necessary.

Author Contributions: Data curation, K.J.D.; Formal analysis, V.G.; Methodology, W.H.; Resources, K.J.D., W.H., J.S., B.G. and J.W.; Supervision, V.G., M.M., S.S., W.H., J.S., J.M. and A.S.; Writing—original draft, K.J.D.; Writing—review & editing, K.J.D., V.G., W.H. and J.S. All authors have read and agreed to the published version of the manuscript.

Funding: This research was funded by the Ministerium für Wissenschaft, Forschung und Kunst Baden-Württemberg (Ministry of Science, Research and the Arts of the state of Baden-Württemberg) within the Nachhaltigkeitsförderung (sustainability support) of the projects of the Exzellenzinitiative I, and also by the DFG-Deutsche Forschungsgemeinschaft (German Research Foundation), in the framework of project MA 1280/57-1.

Data Availability Statement: Not applicable.

Acknowledgments: This research was funded by the Ministerium für Wissenschaft, Forschung und Kunst Baden-Württemberg (Ministry of Science, Research and the Arts of the state of Baden-Württemberg) within the Nachhaltigkeitsförderung (sustainability support) of the projects of the Exzellenzinitiative I, and also by the DFG-Deutsche Forschungsgemeinschaft (German Research Foundation), in the framework of project MA 1280/57-1.

Conflicts of Interest: The authors declare no conflict of interest.

References

1. Arregui, I.L. Mechanical Behavior of a Roller Bearing Steel: Strength Differential Effect, Low Temperature Creep and Propagation of Short Cracks. Ph.D. Thesis, KTH School of Engineering Sciences, Department of Solid Mechanics, Royal Institute of Technology, Stockholm, Sweden, 2015.
2. Spriestersbach, D.; Grad, P.; Kerscher, E. Crack Initiation Mechanisms and Threshold Values of Very High Cycle Fatigue Failure of High Strength Steels. *Procedia Eng.* **2014**, *74*, 84–91. [[CrossRef](#)]
3. Beswick, J.M. Fracture and fatigue crack propagation properties of hardened 52100 steel. *Met. Mater. Trans. A* **1989**, *20*, 1961–1973. [[CrossRef](#)]
4. Lundberg, G.; Palmgren, A. Dynamic Capacity of Rolling Bearings. *J. Appl. Mech.* **1949**, *16*, 165–172. [[CrossRef](#)]
5. Ioannides, E.; Harris, T.A. A New Fatigue Life Model for Rolling Bearings. *J. Tribol.* **1985**, *107*, 367–377. [[CrossRef](#)]
6. Sadeghi, F.; Jalalahmadi, B.; Slack, T.S.; Raje, N.; Arakere, N.K. A Review of Rolling Contact Fatigue. *J. Tribol.* **2009**, *131*, 041403. [[CrossRef](#)]
7. Walvekar, A.A.; Paulson, N.; Sadeghi, F.; Weinzapfel, N.; Correns, M.; Dinkel, M. A New Approach for Fatigue Damage Modeling of Subsurface-Initiated Spalling in Large Rolling Contacts. *J. Tribol.* **2016**, *139*, 011101. [[CrossRef](#)]
8. Spille, J.; Wranik, J.; Barteldes, S.; Mayer, J.; Schwedt, A.; Zürcher, M.; Lutz, T.; Wang, L.; Holweger, W. A study on the initiation processes of white etching cracks (WECs) in AISI 52100 bearing steel. *Wear* **2021**, *477*, 203864. [[CrossRef](#)]
9. Holweger, W.; Wolf, M.; Merk, D.; Blass, T.; Goss, M.; Loos, J.; Barteldes, S.; Jakovics, A. White etching crack root cause investigations. *Tribol. Trans.* **2015**, *58*, 59–69. [[CrossRef](#)]
10. Holweger, W.; Schwedt, A.; Rumpf, V.; Mayer, J.; Bohnert, C.; Wranik, J.; Spille, J.; Wang, L. A Study on Early Stages of White Etching Crack Formation under Full Lubrication Conditions. *Lubricants* **2022**, *10*, 24. [[CrossRef](#)]
11. Murakami, Y.; Norikura, T.; Yasuda, T. Stress intensity factors for a penny-shaped crack emanating from an ellipsoidal cavity. *Trans. JSME* **1982**, *48*, 1558–1565. [[CrossRef](#)]
12. Lai, J.; Lund, T.; Rydén, K.; Gabelli, A.; Strandell, I. The fatigue limit of bearing steels—Part I: A pragmatic approach to predict very high cycle fatigue strength. *Int. J. Fatigue* **2012**, *38*, 155–168. [[CrossRef](#)]
13. Paris, P.; Erdogan, F. A critical analysis of crack propagation laws. *J. Basic Eng.* **1963**, *85*, 528–533. [[CrossRef](#)]
14. Kruhoffer, W.; Loos, J. WEC formation in rolling bearings under mixed friction: Influence and ‘friction energy accumulation’ as indicator. *Tribol. Trans.* **2017**, *60*, 516–529. [[CrossRef](#)]
15. Manieri, F.; Stadler, K.; Morales-Espejel, G.E.; Kadiric, A. The origin of white etching cracks and their significance to rolling bearing failures. *Int. J. Fatigue* **2019**, *120*, 107–133. [[CrossRef](#)]
16. Richardson, A.D.; Evans, M.H.; Wood, R.J.; Ingram, M.; Meuth, B. The evaluation of white etching cracks (WECs) in rolling contact fatigue-tested 100Cr6 steel. *Tribol. Trans.* **2018**, *66*, 6.
17. Rumpf, V. A Study on Microstructural Alterations in White Etching Cracks, Dark Etching Region, and White Etching Bands in Rolling Contacts. Ph.D. Thesis, Faculty of Engineering and the Environment, National Centre for Advanced Tribology at Southampton (nCATS), University of Southampton, Southampton, UK, May 2018.
18. Kerscher, E.; Lang, K.-H. Influence of thermal and thermomechanical treatments on the fatigue limit of a bainitic high-strength bearing steel. *Procedia Eng.* **2010**, *2*, 1731–1739. [[CrossRef](#)]
19. Kunz, L.; Lukas, P.; Cincala, M.; Nicoletto, G. Fatigue Lifetime of Bearing Steel in Ultra-High-Cycle Region. In *Fracture of Nano and Engineering Materials and Structures*; Gdoutos, E.E., Ed.; Springer: Dordrecht, The Netherlands, 2006.
20. Tanaka, K.; Mura, T. A Dislocation Model for Fatigue Crack Initiation. *J. Appl. Mech.* **1981**, *48*, 97–103. [[CrossRef](#)]
21. Tanaka, K.; Mura, T. A theory of fatigue crack initiation at inclusions. *Met. Mater. Trans. A* **1982**, *13*, 117–123. [[CrossRef](#)]
22. Roos, E.; Eisele, U. Determination of Material Characteristic Values in Elastic-plastic Fracture Mechanics by Means of J-integral Crack Resistance Curves. *J. Test. Eval.* **1988**, *16*, 1–11.
23. Monnet, G.; Pouchon, M.A. Determination of the critical resolved shear stress and the friction stress in austenitic stainless steels by compression of pillars extracted from single grains. *Mater. Lett.* **2013**, *98*, 128–130. [[CrossRef](#)]
24. Mlikota, M.; Schmauder, S.; Božić, Z. Calculation of the Wöhler (S-N) curve using a two-scale model. *Int. J. Fatigue* **2018**, *114*, 289–297. [[CrossRef](#)]
25. Mlikota, M.; Schmauder, S.; Božić, Z.; Hummel, M. Modelling of overload effects on fatigue crack initiation in case of carbon steel. *Fatigue Fract. Eng. Mater. Struct.* **2017**, *40*, 1182–1190. [[CrossRef](#)]
26. Mlikota, M.; Schmauder, S. On the Critical Resolved Shear Stress and its Importance in the Fatigue Performance of Steels and other Metals with Different Crystallographic Structures. *Metals* **2018**, *8*, 883. [[CrossRef](#)]
27. Mlikota, M.; Schmauder, S. Virtual testing of plasticity effects on fatigue crack initiation. In *Advances in Engineering Materials, Structures and Systems: Innovations, Mechanics and Applications*; Zingoni, A., Ed.; CRC Press: London, UK, 2019; pp. 587–592.
28. Mlikota, M.; Staib, S.; Schmauder, S.; Božić, Ž. Numerical determination of Paris law constants for carbon steel using a two-scale model. *J. Phys. Conf. Ser.* **2017**, *843*, 012042. [[CrossRef](#)]
29. Mlikota, M.; Schmauder, S. Numerical determination of component Wöhler curve. *DVM Bericht* **2017**, *1684*, 111–124.

30. Božić, Ž.; Schmauder, S.; Mlikota, M.; Hummel, M. Multiscale fatigue crack growth modeling for welded stiffened panels. In *Handbook of Mechanics of Materials*; Schmauder, S., Chen, C.-S., Chawla, K.K., Chawla, N., Chen, W., Kagawa, Y., Eds.; Springer: Singapore, 2018; pp. 1–21.
31. Božić, Ž.; Schmauder, S.; Mlikota, M. Application of the DK, DJ and DCTOD parameters in fatigue crack growth modelling. *Tech. Gaz.* **2011**, *18*, 459–466.
32. Božić, Ž.; Schmauder, S.; Mlikota, M. Fatigue growth models for multiple long cracks in plates under cyclic tension based on DKI, DJ-integral and DCTOD parameter. *Key Eng. Mater.* **2011**, *488*, 525–528. [[CrossRef](#)]
33. Anderson, J. The influence of grain size variation on metal fatigue. *Int. J. Fatigue* **2005**, *27*, 847–852. [[CrossRef](#)]
34. Simonovski, I.; Cizelj, L. The influence of grains' crystallographic orientations on advancing short crack. *Int. J. Fatigue* **2007**, *29*, 2005–2014. [[CrossRef](#)]
35. Newman, J.; Phillips, E.; Swain, M. Fatigue-life prediction methodology using smallcrack theory. *Int. J. Fatigue* **1999**, *21*, 109–119. [[CrossRef](#)]
36. Zavadzka, D.; Tillova, E.; Guagliano, M.; Chalupova, M.; Kucharikova, L. Effect of porosity on the fatigue behavior of AlZn10Si8Mg casting alloys in a high cycle region. *Procedia Eng.* **2017**, *192*, 988–993. [[CrossRef](#)]
37. Osmond, P.; Le, V.D.; Morel, F.; Bellett, D.; Saintier, N. Effect of porosity on the fatigue strength of cast aluminum alloys: From the specimen to the structure. *Procedia Eng.* **2018**, *213*, 630–643. [[CrossRef](#)]